

Anion Exchange Promoting Non-Impurities Enables Conformable and Efficient Inverted Perovskite Solar Cells

Jun Fang^{1†}, Dongxu Lin^{1†}, Guanshui Xie¹, Sibao Li¹, Huan Li¹, Xin Wang¹, Daozeng Wang¹, Nuanshan Huang¹, Haichen Peng¹, Lin Gan¹, Yanzhuo Zhu¹, Sisi He² and Longbin Qiu^{1*}

¹Shenzhen Key Laboratory of Intelligent Robotics and Flexible Manufacturing Systems, Department of Mechanical and Energy Engineering, SUSTech Energy Institute for Carbon Neutrality, Southern University of Science and Technology, Shenzhen, 518055, China

²Shenzhen Key Laboratory of Flexible Printed Electronics Technology, School of Science, Harbin Institute of Technology (Shenzhen), University Town, Shenzhen, Guangdong, 518055, China

*Corresponding author: Longbin Qiu, Email: qiulb@sustech.edu.cn.

† These authors contributed equally to this work.

Experimental Section

Materials

Formamidinium iodide (FAI), formamidinium bromide (FABr), methylammonium iodide (MAI), methylammonium bromide (MABr) and methylammonium chloride (MACl) were purchased from Greatcell Solar Materials. Lead iodide (PbI_2 , 99.999%), [2-(3,6-dimethoxy-9H-carbazol-9-yl) ethyl] phosphonic acid (MeO-2PACz), and [4-(3,6-dimethoxy-9H-carbazol-9-yl) butyl] phosphonic acid (Me-4PACz) were purchased from TCI. Phenethylammonium bromide (PEABr), fullerene (C_{60}) and bathocuproine (BCP) were purchased from Xi'an Polymer Light Technology. Phenyl-C₆₁-butyric acid methyl-ester (PC_{61}BM) were purchased from Advanced Election Technology. Isopropanol (IPA) was purchased from thermos scientific. Chlorobenzene (CB) was purchased from Sigma Aldrich. Ethyl alcohol was purchased from Aladdin. All chemicals were used as received.

Perovskite solar cells fabrication

Perovskite film prepared by thermal evaporation-blade process

PbI_2 with a thickness of 250 nm was deposited at 5 Å/s in a high-vacuum ($<5 \times 10^{-4}$ Pa) chamber (Wuhan PUDI Vacuum). For FAMAPbI perovskite film deposition, an organic salt solution of FAI: MAI (0.407 mmol: 0.166 mmol in 1 mL IPA) was blade-coated onto PbI_2 layers in ambient air (model of blade-coater: LEBO SCIENCE PF200-H), followed by annealing at 150 °C for 15 min. For FAMAPbI-Cl perovskite film deposition, an organic salt solution of FAI: MAI: MACl (0.407 mmol: 0.062 mmol: 0.104 mmol in 1 mL IPA) was blade-coated onto PbI_2 layers in ambient air, followed by annealing at 150 °C for 15 min. For FAMAPbI-BrCl perovskite film deposition, an organic salt solution of FAI: MABr: MACl (0.407 mmol: 0.062 mmol: 0.104 mmol in 1 mL IPA) was blade-coated onto PbI_2 layers in ambient air, followed by annealing at 150 °C for 15 min. For FAPbI-BrCl perovskite film deposition, an organic salt solution of FAI: FABr: MACl (0.407 mmol: 0.062 mmol: 0.104 mmol in 1 mL IPA) was blade-

coated onto PbI₂ layers in ambient air, followed by annealing at 150 °C for 15 min.

Perovskite film prepared by thermal evaporation-spin process

PbI₂ with a thickness of 250 nm was deposited at 5 Å/s in a high-vacuum ($<5 \times 10^{-4}$ Pa) chamber. For FAMAPbI perovskite film deposition, an organic salt solution of FAI: MAI (0.407 mmol: 0.166 mmol in 1 mL IPA) was spin-coated onto PbI₂ layers at 2,000 rpm for 30 s (model of spin-coater: LEBO SCIENCE EZ6-S), followed by annealing at 150 °C for 15 min. For FAMAPbI-Cl perovskite film deposition, an organic salt solution of FAI: MAI: MACl (0.407 mmol: 0.062 mmol: 0.104 mmol in 1 mL IPA) was spin-coated onto PbI₂ layers at 2,000 rpm for 30 s, followed by annealing at 150 °C for 15 min. For FAMAPbI-BrCl perovskite film deposition, an organic salt solution of FAI: MABr: MACl (0.407 mmol: 0.062 mmol: 0.104 mmol in 1 mL IPA) was spin-coated onto PbI₂ layers at 2,000 rpm for 30 s, followed by annealing at 150 °C for 15 min.

Perovskite solar cells and modules fabrication

For perovskite solar cells, ITO glass was sequentially washed with detergent, distilled water, acetone and IPA for 20 mins. Before use, the ITO glass was dried and treated by ultraviolet ozone for 30 mins to improve the surface wetting properties. For hole transport materials (HTM) solution, The MeO-2PACz or Me-4PACz solution was dissolved in ethyl alcohol with a concentration of 1 mg/mL. The 100 µL of HTM solution was spin-coated on the cleaned ITO substrates at 3000 rpm for 30 s and annealed at 100 °C for 10 min. The perovskite film was deposited on the ITO/HTM substrate via the above fabrication methods. For surface passivation, the as-prepared PEABr solution was spin-coated on the top of perovskite film at 5000 rpm for 30 s. Afterwards, the PCBM solution (10 mg/mL dissolved in CB) was spin-coated on the ITO/HTM/Perovskite/PEABr films at 3000 rpm for 30 s. Finally, the 10 nm C₆₀, 5 nm BCP, and 90 nm Ag were thermally evaporated at 0.1-1.0 Å/s in a high-vacuum ($<5 \times 10^{-4}$ Pa) chamber to obtain the complete devices. The antireflection film (Mitsubishi)

was used to enhance the light absorption. For perovskite solar module, the fabrication is analogous to that of small-area solar cells except the amount of solution used in the preparing process, the size of glass/ITO substrate and laser scribing patterning procedure. More dosage of solution is needed to completely cover the $5 \times 5 \text{ cm}^2$ substrate. The perovskite solar module active area was 12.6 cm^2 .

Characterizations

The X-ray diffractometer (XRD) patterns, grazing incidence X-ray diffraction (GIXRD) patterns, and the in situ XRD patterns were carried out by using a Rigaku Smartlab equipped with Cu K α radiation in the 2θ range of $3\text{-}65^\circ$ at a scanning rate of $10^\circ/\text{min}$. The wavelength (λ) of incident X-ray is 1.5418 \AA . The grazing-incidence wide-angle X-ray scattering (GIWAXS) measurements were performed at BL02U2 beamline of the Shanghai Synchrotron Radiation Facility (SSRF). The scanning electron microscope (SEM) images energy dispersive X-ray spectroscopy (EDX) were obtained from Merlin field emission SEM at an acceleration voltage of 2-3 kV and a current of 25-50 pA. The photoluminescence (PL) spectra and time-resolved PL (TRPL) were performed using an Edinburgh Instrument FLS1000 system applying a 450 nm laser as the excitation source. The perovskite samples were coated on the ITO substrates. The decay lifetime was obtained by fitting the formula of $f(t) = y_0 + A_1 \exp^{-t/\tau_1} + A_2 \exp^{-t/\tau_2}$ using biexponential decay model. A_1 , and A_2 are constants associated with baseline offset and the contributions of fast (τ_1) and slow (τ_2) segments, respectively. The average carrier lifetime (τ_{ave}) can be determined from the equation of $\tau_{ave} = \frac{\sum A_i \tau_i^2}{\sum A_i \tau_i}$. The chi-square value ($\chi^2 = \sum \frac{(\text{Observed value} - \text{Expected value})^2}{\text{Expected value}}$) represents the reliability of fitting curves. The PL mapping images were obtained from confocal laser scanning fluorescence microscope (Leica, TCS SP8). Time-of-flight secondary ion mass spectrometry (ToF-SIMS) was carried out on a Nano ToF 2 instrument (ULVAC-PHI, Japan) equipped with bismuth as primary ion source. The ToF-SIMS data was acquired on the area of $100 \times 100 \mu\text{m}^2$ by using a 30 keV Bi primary ion beam, followed by a 3 second/cycle sputter of a

400×400 μm² area using 3 keV Ar ion beams. Sputter rate is 0.3 nm/s (Ar⁺) for SiO₂. The UV-vis absorption spectra and in situ UV-vis absorption spectra were carried out in air by using UV-vis spectroscopy (HITACHI, UH5700). The roughness of the films was collected from the atomic force microscope (AFM) (MFP-3D Stand Alone). The photocurrent density-voltage (*J-V*) curves of the PSCs were measured using a solar simulator (Sol3A Class AAA, Oriel, Newport, USA) and a Keithley 2420 source meter. The devices were tested under AM 1.5G sun illumination (100 mW/cm²). A standard reference silicon cell (91150-KG3, Newport, USA) was used to calibrate the light intensity. The metal masks of 0.1 cm² was employed to determine the active area of the PSCs. The reverse scan range is from 1.2 V to 0 V and the forward scan range is from 0 V to 1.2 V. The current-voltage scan speed is 0.2 V/s and dwell time is 30 ms. The testing environmental conditions is in the ambient air with relative humidity of 60-80%. The incident photon to converted electron efficiency (IPCE) measurement was conducted to obtain the external quantum efficiency (EQE) spectra with a range from 400 to 900 nm using EQE system (IQE 200B, Newport). The electroluminescence (EL) spectra were characterized by a Keithley 2420 source meter and integrating sphere connected to a spectrophotometer (QE65Pro). The voltage loss induced by the non-radiative recombination was calculated from the equation of $\Delta V_{OC}^{nonrad} = -\frac{k_B T}{q} \ln(EQE_{EL})$, where k_B , T , q , and EQE_{EL} are electron charge, Boltzmann constant, temperature and the electroluminescence efficiency. For the measurement of open-circuit voltage under different light intensities, the relationship between open-circuit voltage and light intensity could be described by the formula of $qV_{OC} = E_g + n_{ID} k_B T \ln \frac{I}{I_0}$, where q , k_B , T , I , E_g stand for electron charge, the Boltzmann constant, the absolute temperature, light intensity and optical bandgap of perovskite, respectively. For the long-term stability measurement, a white light LED with the intensity calibrated to satisfy one-sun conditions was used as the illumination source. The PSCs were put into a homemade box sealed and supplied with continuous N₂ flowing to control the relative humidity of ambient condition. For the storage stability measurement, the PSCs

without encapsulation were stored in a nitrogen-filled glovebox.

Section SI: Effect of anion-exchange on perovskite film growth



Figure S1. Photographs of the perovskite films before annealing **a.** FAMAPbI and **b.** FAMAPbI-Cl **c.** FAMAPbI-BrCl. The scale bar is 5 mm.

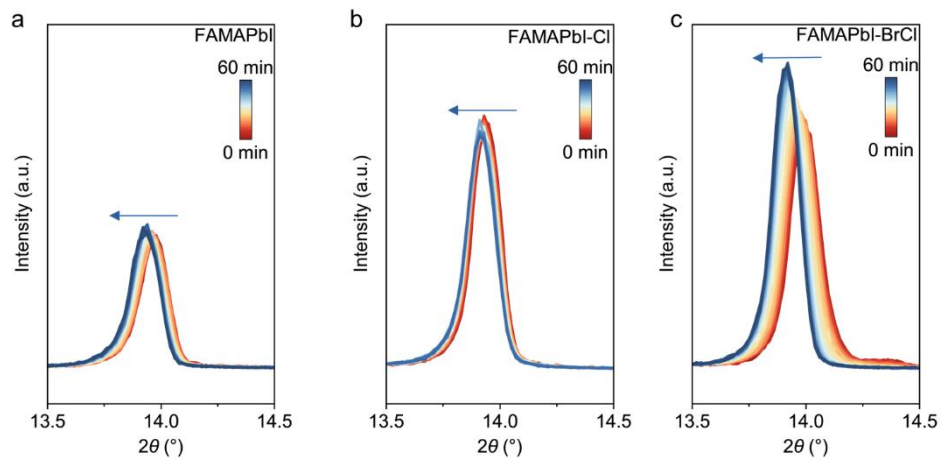


Figure S2. *In-situ* XRD showing diffraction peak as a function of the annealing time for **a.** FAMAPbI, **b.** FAMAPbI-Cl, and **c.** FAMAPbI-BrCl perovskite films.

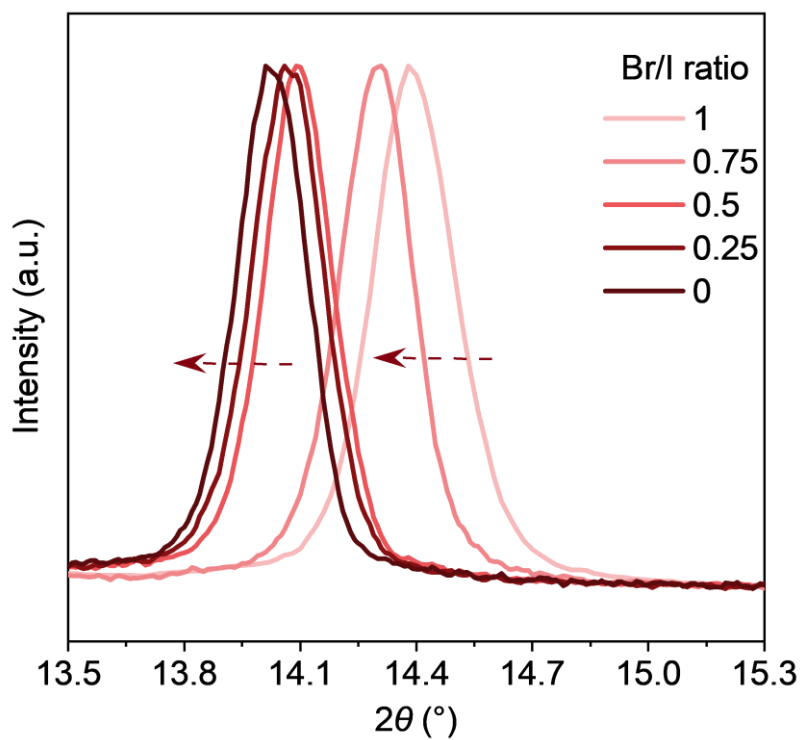


Figure S3. The (100) peak crystal planes of XRD pattern for perovskite films with the different MABr/MAI ratios.

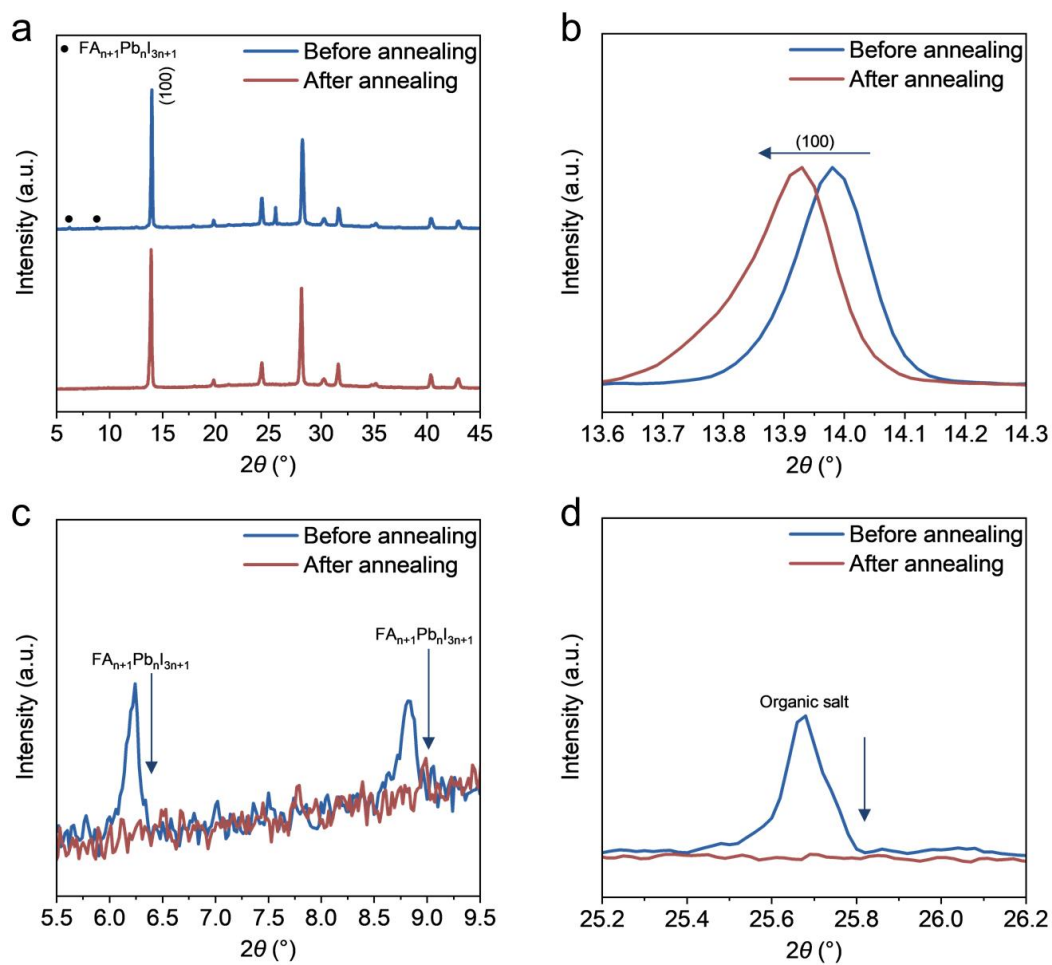


Figure S4. a. XRD pattern and b-d. magnified XRD patterns of the FAMAPbI-BrCl perovskite film before and after annealing in ambient air.

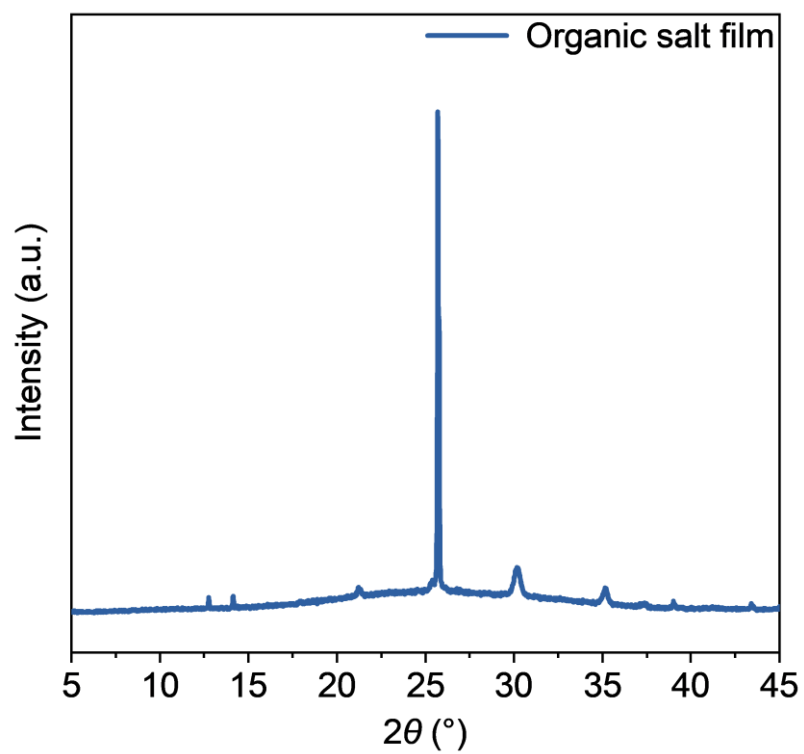


Figure S5. XRD pattern of the blade-coated organic salt film.

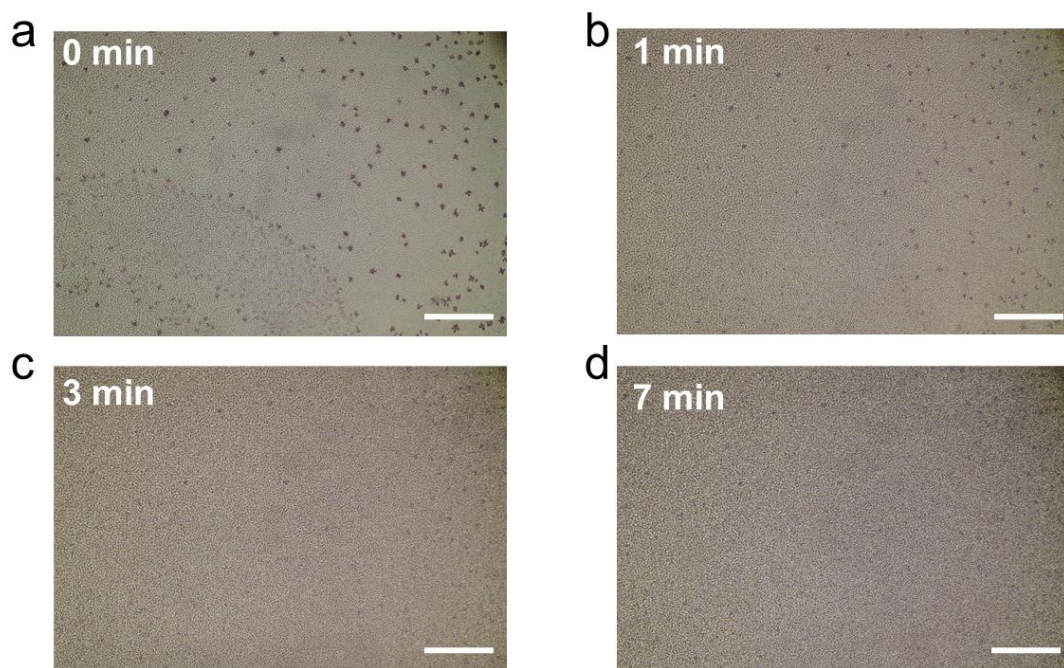


Figure S6. Time-dependent morphological evolution of FAMAPbI-BrCl perovskite film during the thermal annealing process. The scale bar is 100 μm .

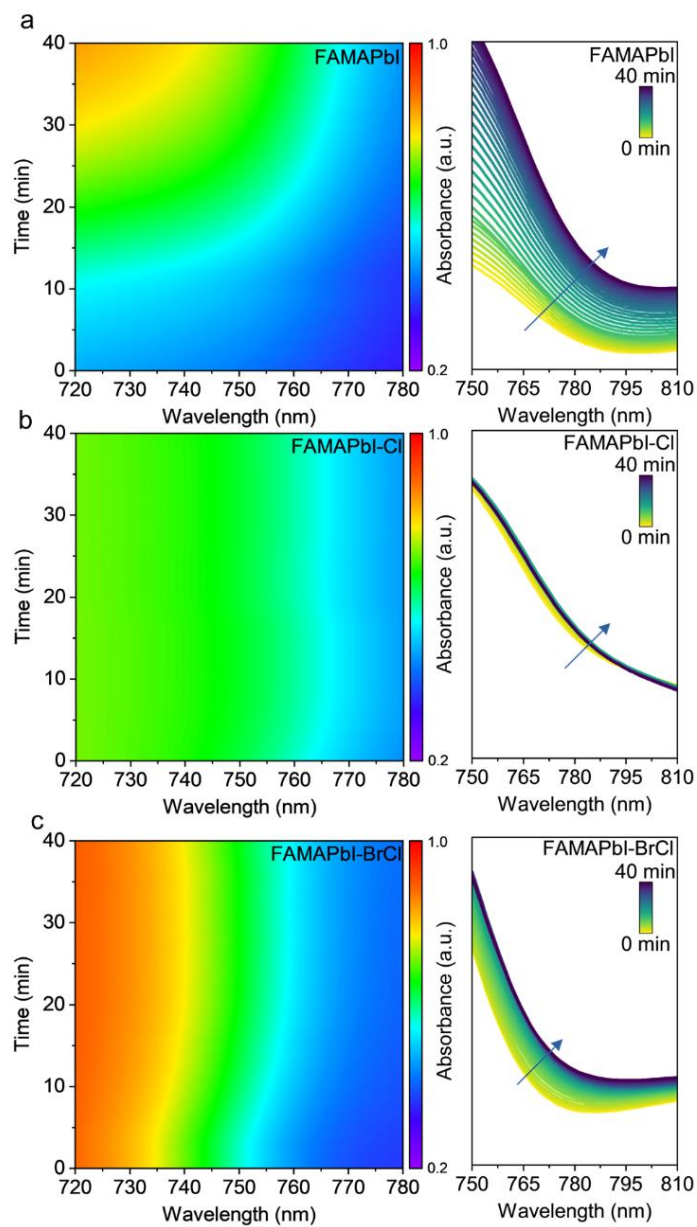


Figure S7. *In-situ* UV-vis absorption spectra during the annealing process based on **a.** FAMAPbI, **b.** FAMAPbI-Cl, and **c.** FAMAPbI-BrCl perovskite films.

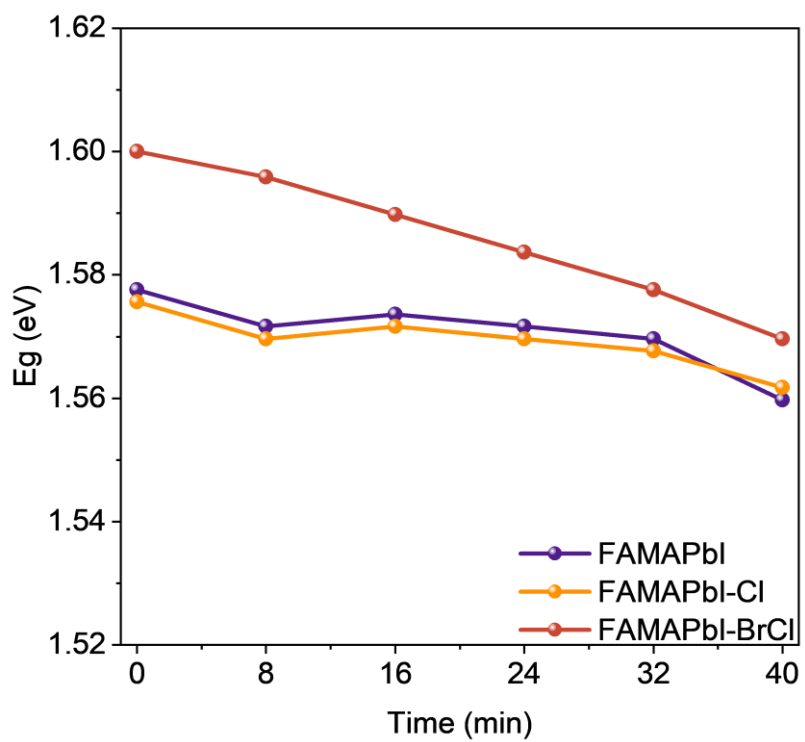


Figure S8. The band gap variation of the corresponding perovskite films during the thermal annealing process.

Section SII: Anion exchange for non-impurities perovskite

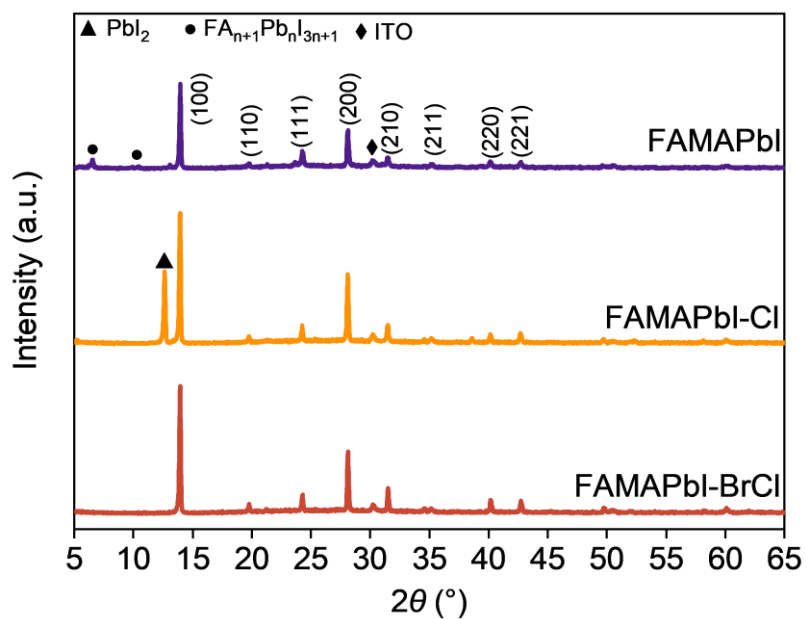


Figure S9. XRD pattern of the perovskite film based on FAMAPbI, FAMAPbI-Cl, and FAMAPbI-BrCl.

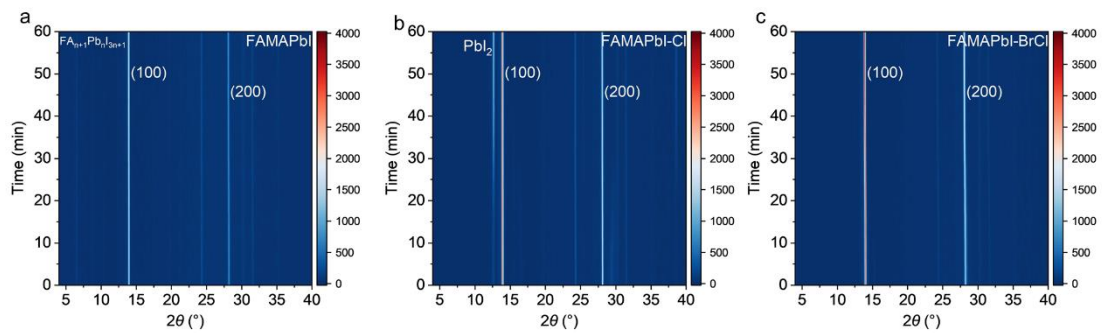


Figure S10. The *in-situ* XRD patterns of **a.** FAMAPbI, **b.** FAMAPbI-Cl, and **c.** FAMAPbI-BrCl perovskite films during the thermal annealing process.

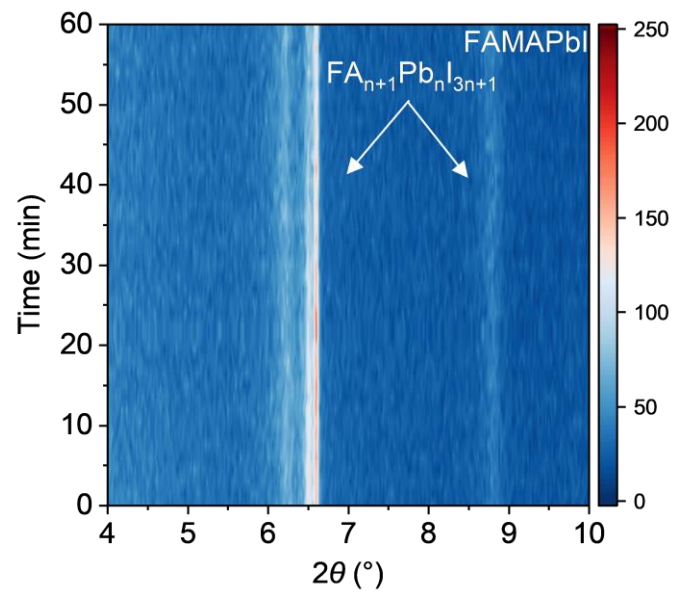


Figure S11. Enlarged image of *in-situ* XRD patterns in **Figure S10a**.

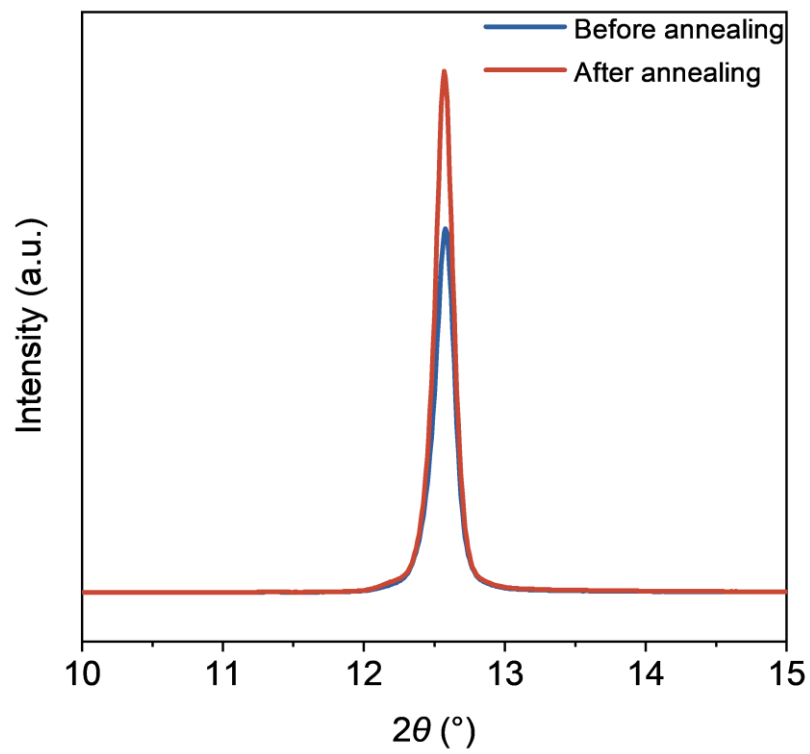


Figure S12. XRD pattern of the PbI₂ film before and after annealing in ambient air.

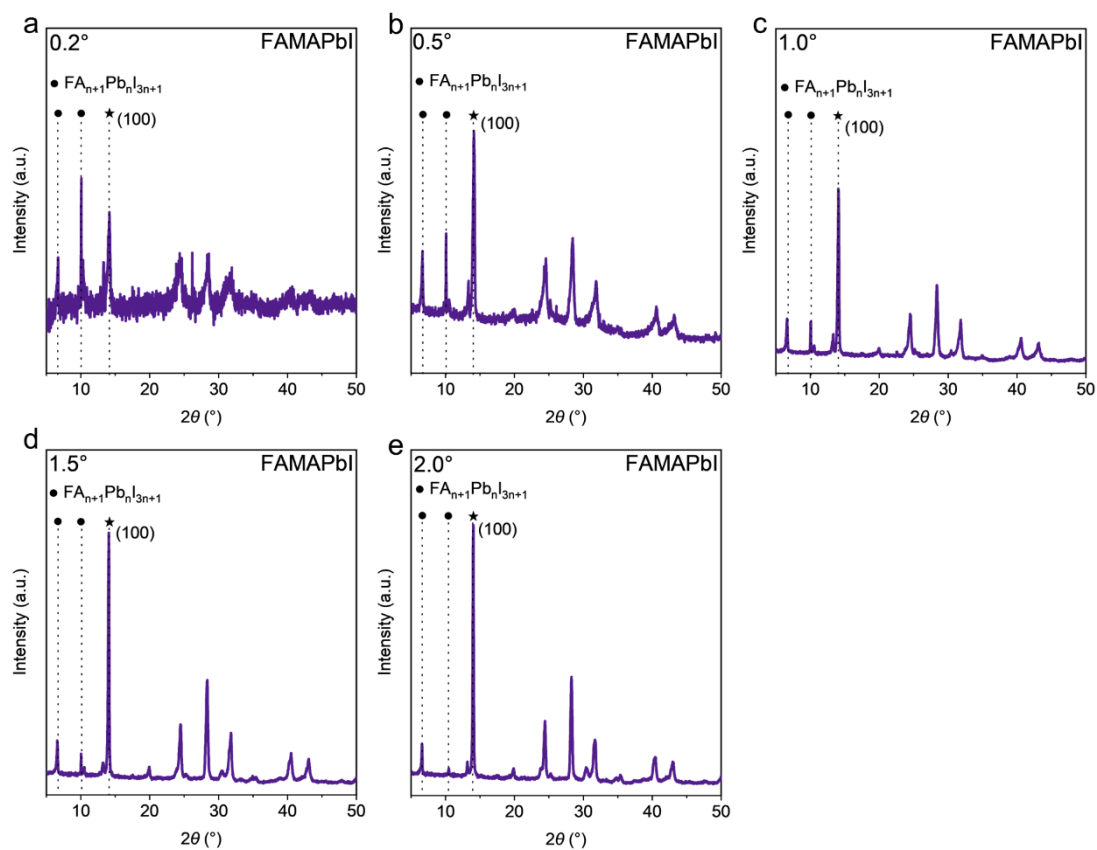


Figure S13. Enlarged XRD patterns of FAMAPbI perovskite film at different incident angles in **Figure 2d**.

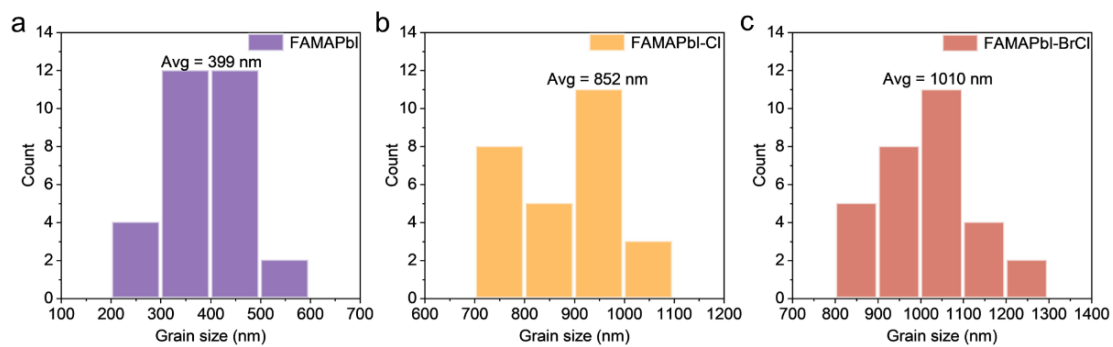


Figure S14. Grain size distributions extracted from the top-view SEM images of **a.** FAMAPbI, **b.** FAMAPbI-Cl, and **c.** FAMAPbI-BrCl perovskite films.

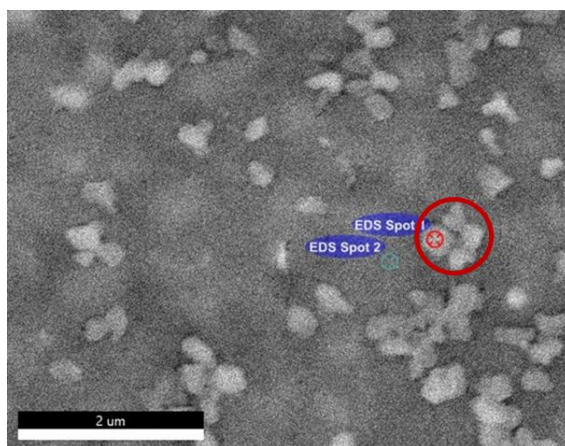


Figure S15. Energy dispersive X-ray spectroscopy (EDS) characterization collected from the white (PbI_2 flakes) and black region (common grain) in the SEM of FAMAPbI-Cl thin film. The element analysis results are summarized in **Table S1** and **S2**, respectively.

Table S1 Data of EDS of position spot 1

Element	Weight percentage	Atomic percentage
C K	8.67	53.26
I L	63.02	36.66
Pb M	28.31	10.08
Total	100	

Table S2 Data of EDS of position spot 2

Element	Weight percentage	Atomic percentage
C K	9.97	56.95
I L	63.25	34.19
Pb M	26.78	8.87
Total	100	

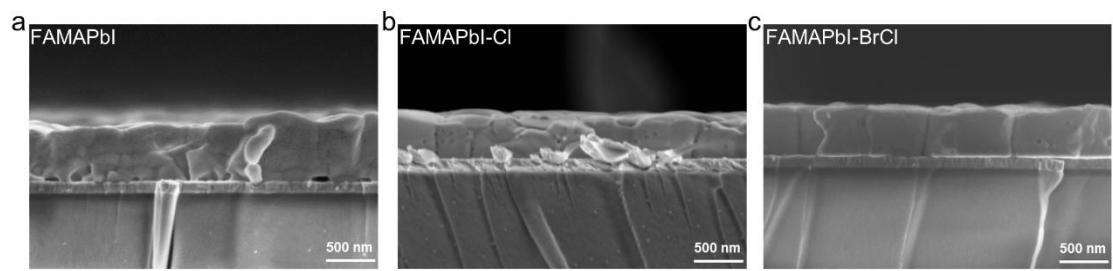


Figure S16. Cross-sectional SEM images of **a.** FAMAPbI, **b.** FAMAPbI-Cl, and **c.** FAMAPbI-BrCl perovskite films.

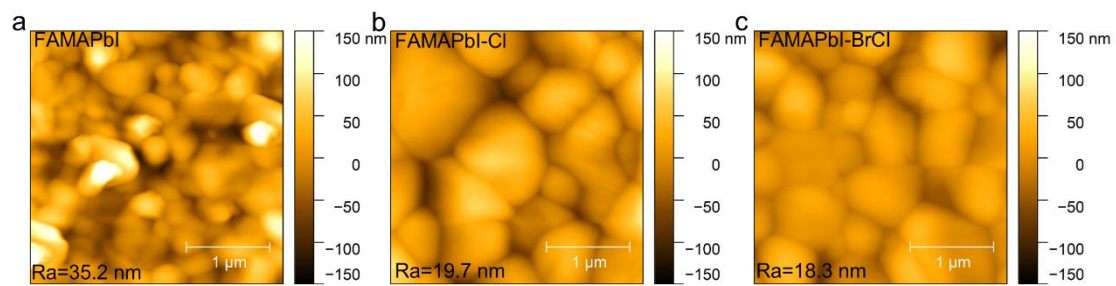


Figure S17. AFM images of **a.** FAMAPbI, **b.** FAMAPbI-Cl, and **c.** FAMAPbI-BrCl perovskite films.

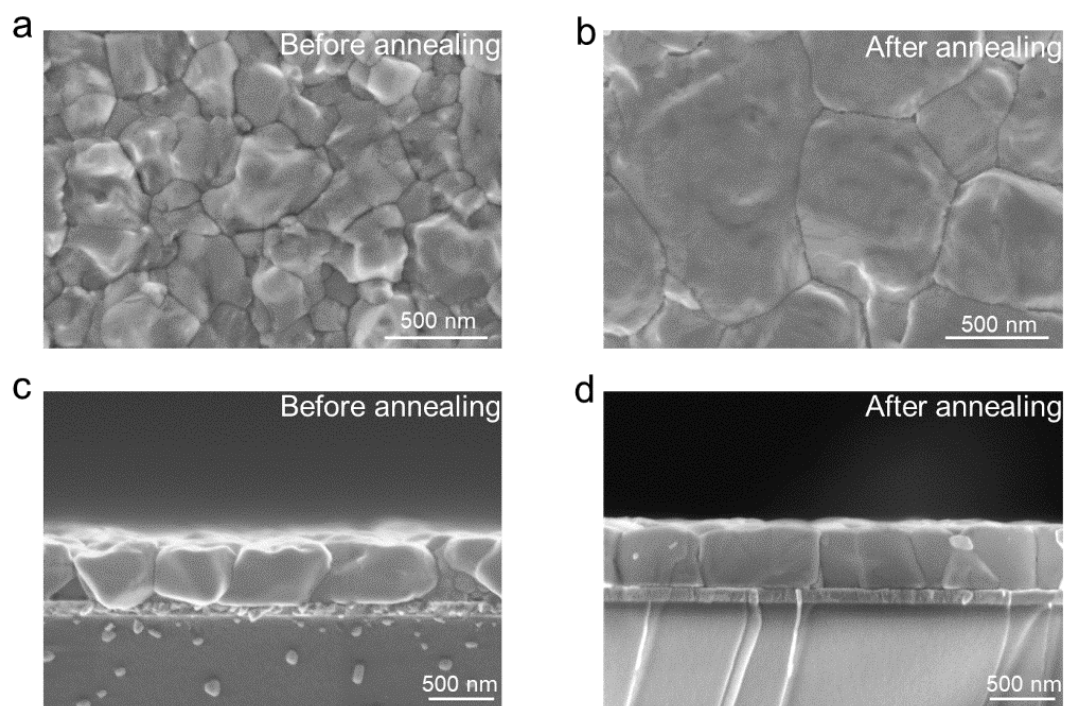


Figure S18. a-b. The top-view SEM images and **c-d.** cross-sectional SEM images of the FAMAPbI-BrCl perovskite film before annealing and after annealing.

Section SIII: Optoelectronic quality of perovskite via anion exchange

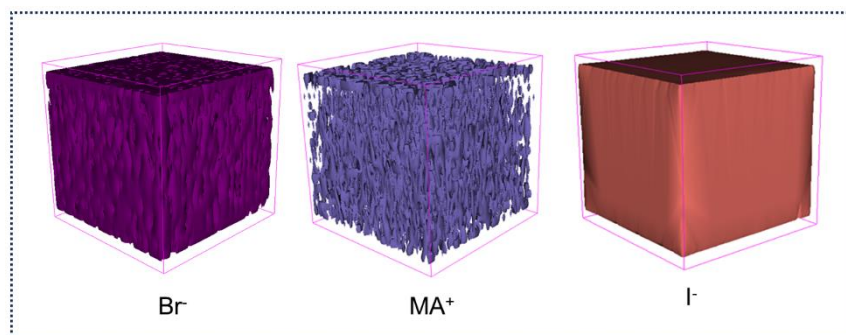


Figure S19. the corresponding ion distribution of Br^- , MA^+ , and I^- SIMS in FAMAPbI-BrCl perovskite film.

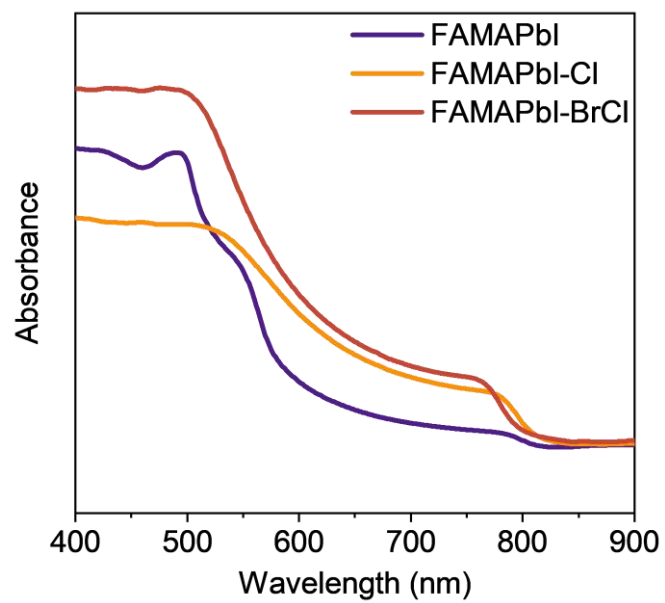


Figure S20. UV-vis absorption spectra of the perovskite film based on FAMAPbI, FAMAPbI-Cl, and FAMAPbI-BrCl.

Section SIV: Photovoltaic performance of perovskite devices via anion exchange

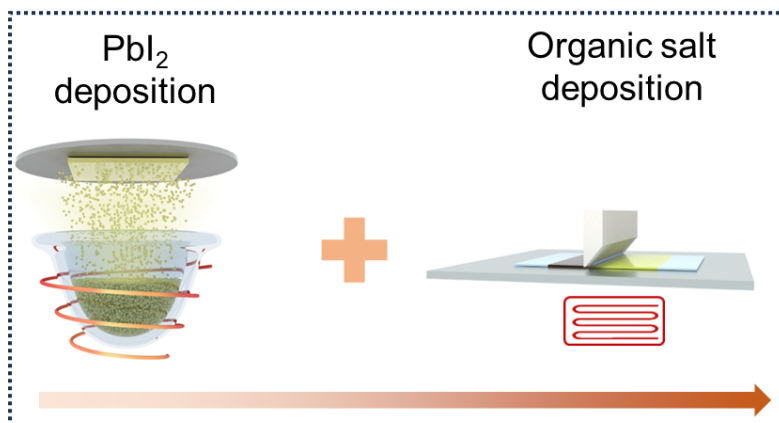


Figure S21. Schematic drawing of the perovskite fabrication via thermal evaporation-blade sequential two-step process.

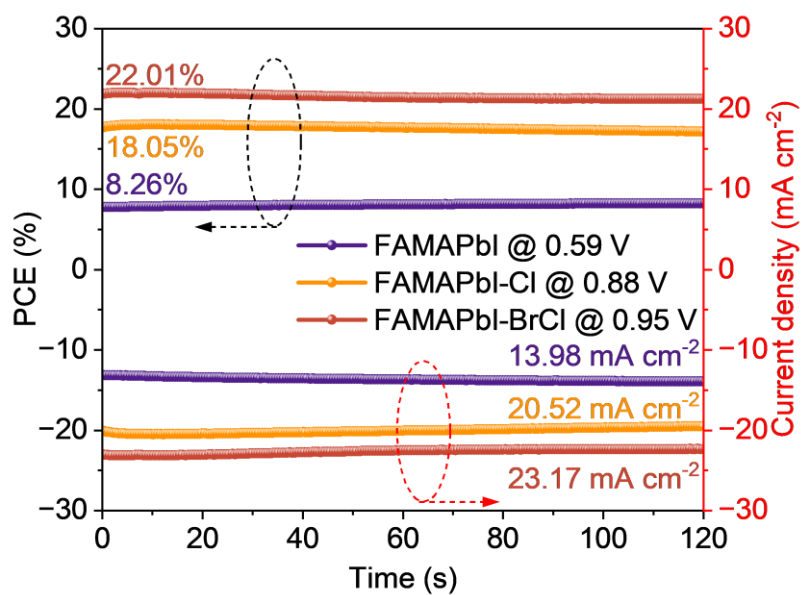


Figure S22. Typical steady-state power output at the initial maximum power point based on the FAMAPbI, FAMAPbI-Cl, and FAMAPbI-BrCl perovskite devices.

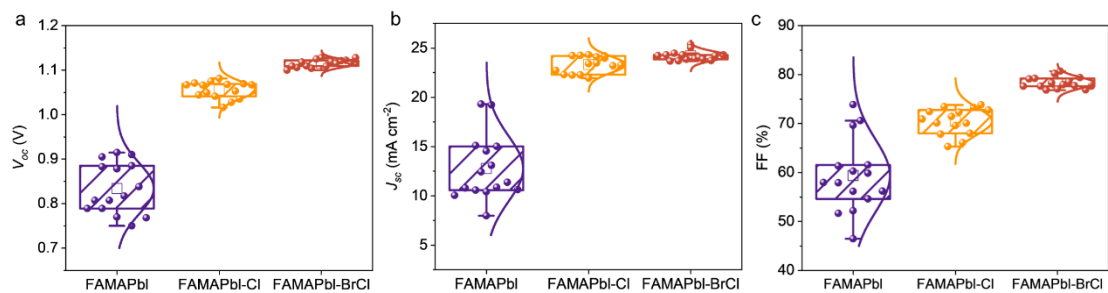


Figure S23. a. V_{oc} b. J_{sc} c. FF statistical distribution of PSCs fabricated by thermal evaporation-blade method.

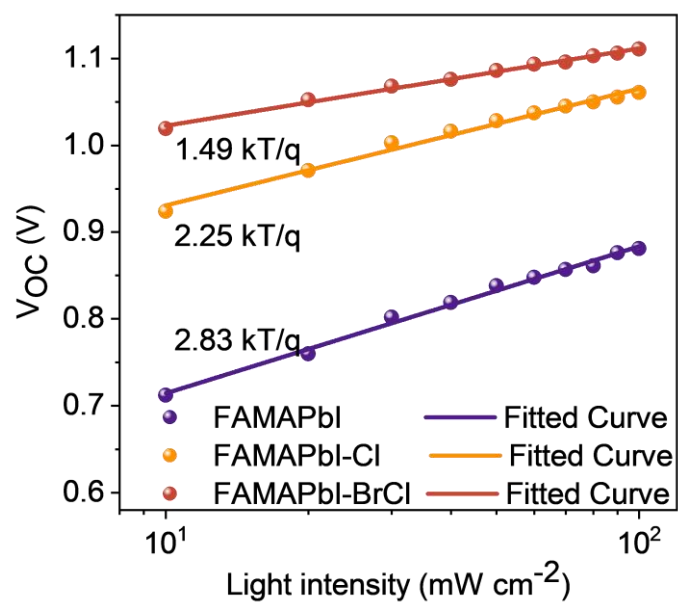


Figure S24. V_{OC} values at various illumination intensities of the inverted PSCs based on the FAMAPbI, FAMAPbI-Cl, and FAMAPbI-BrCl, fabricated by thermal evaporation-blade process.

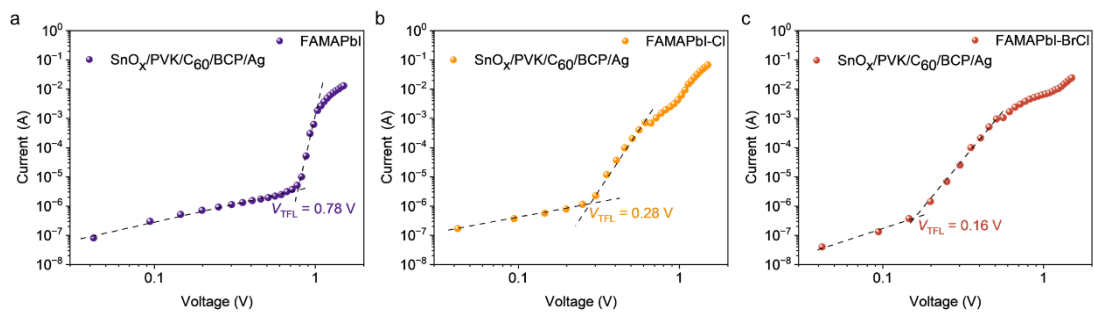


Figure S25. SCLC curves of the electron-only devices for **a.** FAMAPbI, **b.** FAMAPbI-Cl, and **c.** FAMAPbI-BrCl devices.

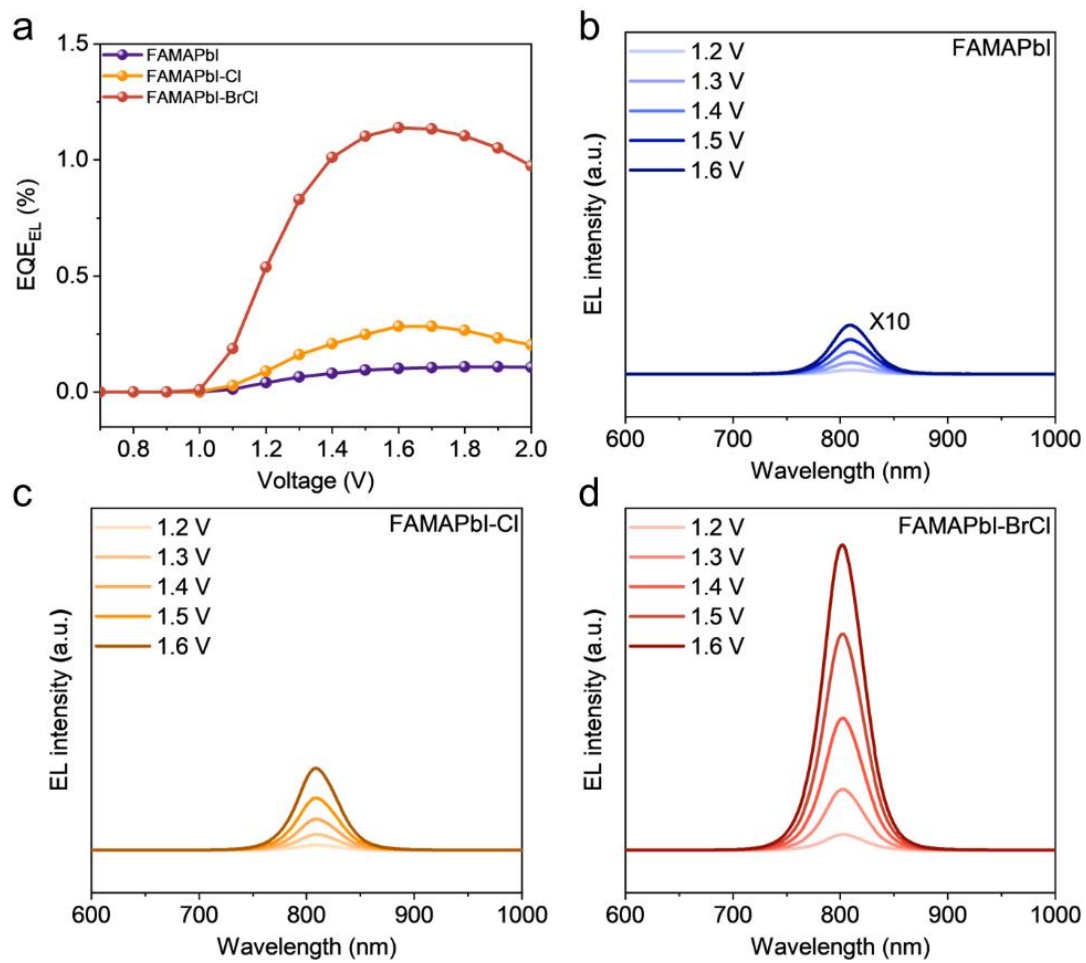


Figure S26. a. The external quantum efficiency of the electroluminescence (EQE_{EL}) as a function of the external voltage, and EL spectra of **b.** FAMAPbI, **c.** FAMAPbI-Cl, and **d.** FAMAPbI-BrCl perovskite devices under different bias voltages.

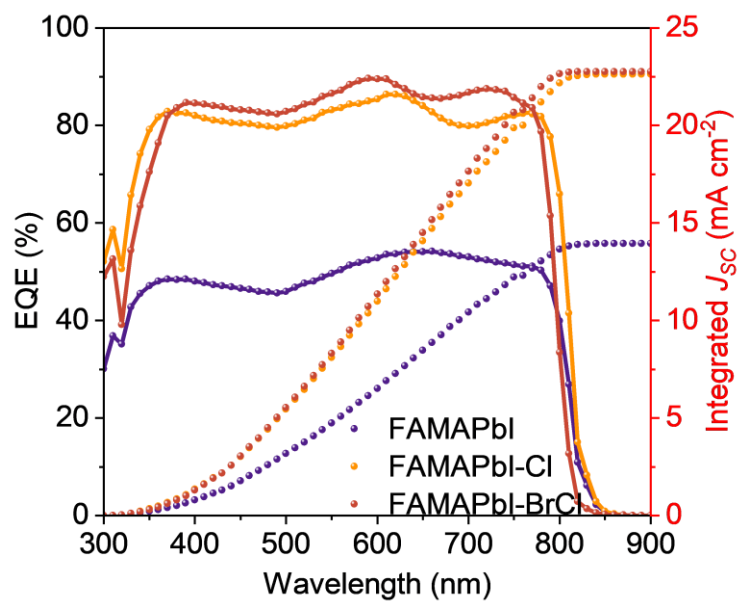


Figure S27. The EQE spectrum and the integrated J_{SC} curves of the inverted PSCs based on the FAMAPbI, FAMAPbI-Cl, and FAMAPbI-BrCl, fabricated by thermal evaporation-blade process.

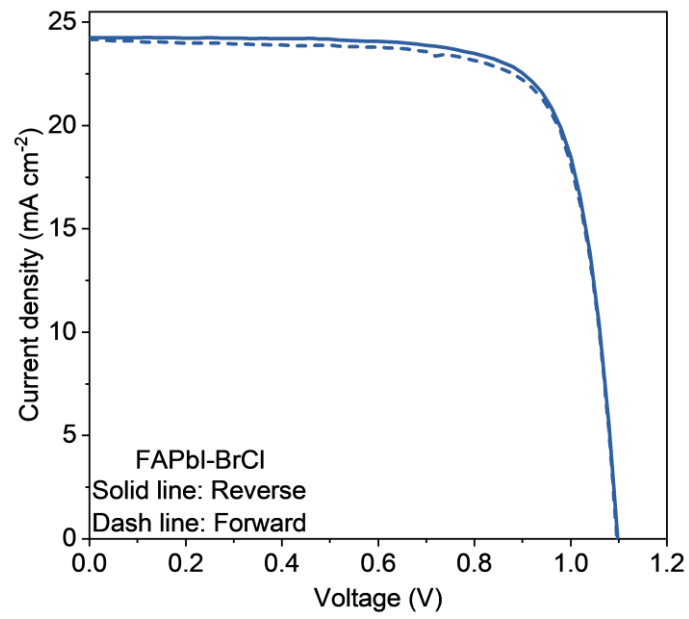


Figure S28. The champion J - V curve of the inverted devices fabricated by thermal evaporation-blade method based on the FAPbI-BrCl.

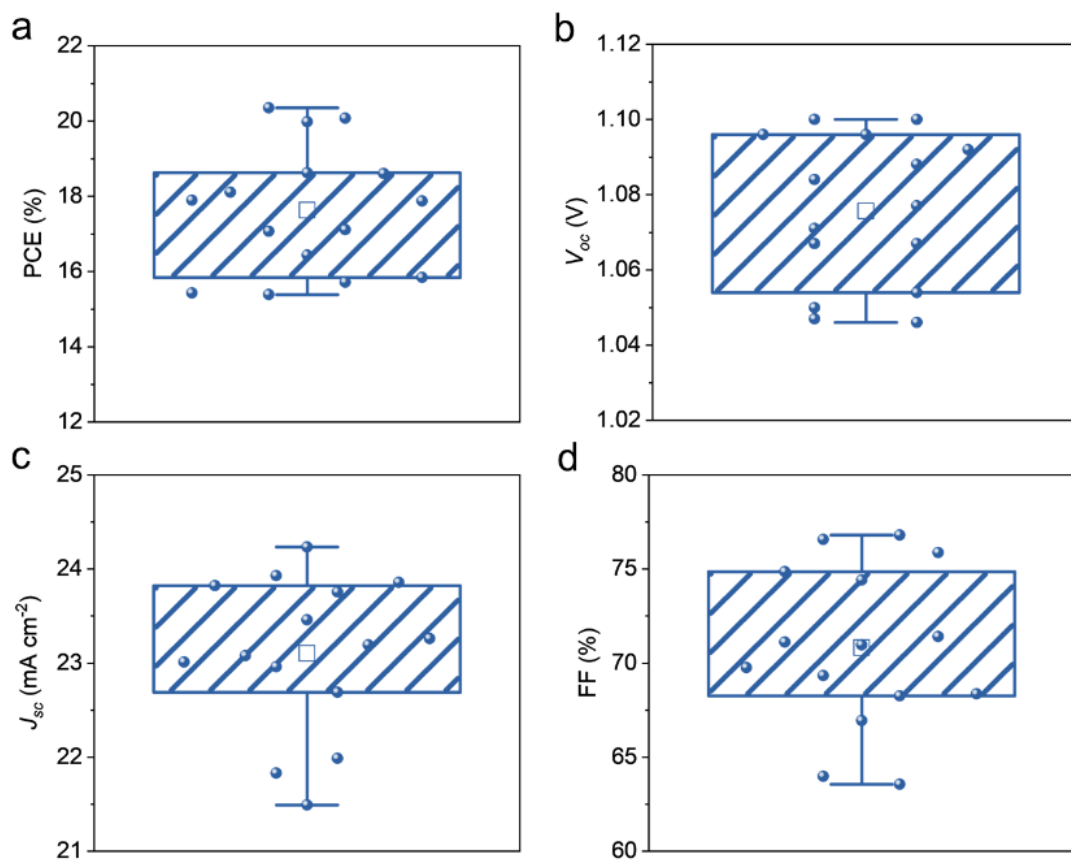


Figure S29. a. PCE b. V_{oc} c. J_{sc} d. FF statistical distribution of PSCs based on the FAPbI-BrCl fabricated by thermal evaporation-blade method.

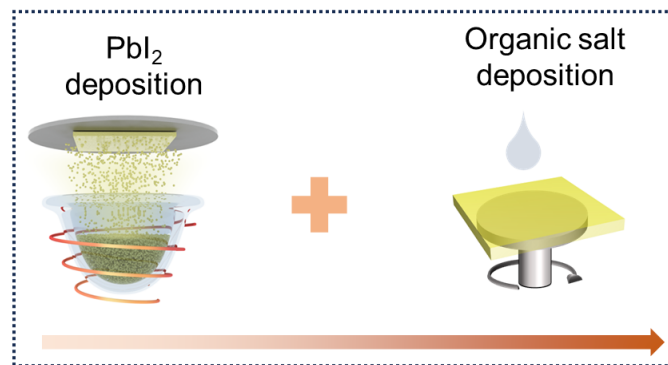


Figure S30. Schematic drawing of the perovskite fabrication via thermal evaporation-spin sequential two-step process.


福建省计量科学研究院
 FUJIAN METROLOGY INSTITUTE
 (国家光伏产业计量测试中心)
 National PV Industry Measurement and Testing Center



检测报告

Test Report

报告编号: 24Q3-00303
Report No.

客户信息	Longbin Qiu Group, Southern University of Science and Technology
联络信息	1088 Xueyuan Avenue, Nanshan District, Shenzhen 518055, China
物品名称	Inverted thermal evaporation-solution processing perovskite solar cell (IV)
型号/规格	1.5cm×1.5cm
物品编号	3-4
制造厂商	Longbin Qiu Group, Southern University of Science and Technology
物品接收日期	2024-05-22
检测日期	2024-05-23

批准人: 蔡健华 蔡健华


核验员: 何翔 何翔

检测员: 陈彩云 陈彩云

发布日期: 2024 年 05 月 29 日



本院/本中心地址: 福州市晋安区9-3号 电话: 0591-87845050 传真: 0591-87808417 邮编: 350003
 Address: 9-3 Pingjiang Road, Fuzhou, China Telephone Fax Post Code
 网站: www.fjil.net 邮编电话: 0591-87845050 投诉电话: 0591-87823035
 Web Site Inquire line Complaint Fax
 未经本院/本中心书面批准, 部分数据不得再行内移/外发。
 Partly using this Report will not be authorized without allowed by FIL Center.


福建省计量科学研究院
 FUJIAN METROLOGY INSTITUTE
 (国家光伏产业计量测试中心)
 National PV Industry Measurement and Testing Center

24Q3-00303

检测结果/说明:
Results of Test and additional explanation.

- Standard Test Condition (STC): Total Irradiance: 1000 W/m²
Temperature: 25.0 °C
Spectral Distribution: AM1.5G
- Measurement Data and I-V/P-V Curves under STC

Forward Scan

I_{sc} (mA)	V_{oc} (V)	I_{mp} (mA)	V_{mp} (V)	P_{MPP} (mW)	FF (%)	A (cm ²)
2.487	1.165	2.300	0.9933	2.285	78.87	0.1012

Reverse Scan

I_{sc} (mA)	V_{oc} (V)	I_{mp} (mA)	V_{mp} (V)	P_{MPP} (mW)	FF (%)	A (cm ²)
2.481	1.173	2.371	1.020	2.418	83.09	0.1012

Mismatch factor: 0.9901

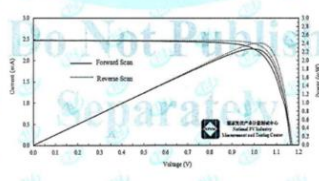


Figure 1. I-V and P-V characteristic curves of the measured sample under STC

检测报告续页专用
Continued page of test report

Figure S31. Certified efficiency of 24.18% for perovskite solar cell with anion exchange in a designated test center National Photovoltaic Industry Metrology and Testing Center (NPVM).

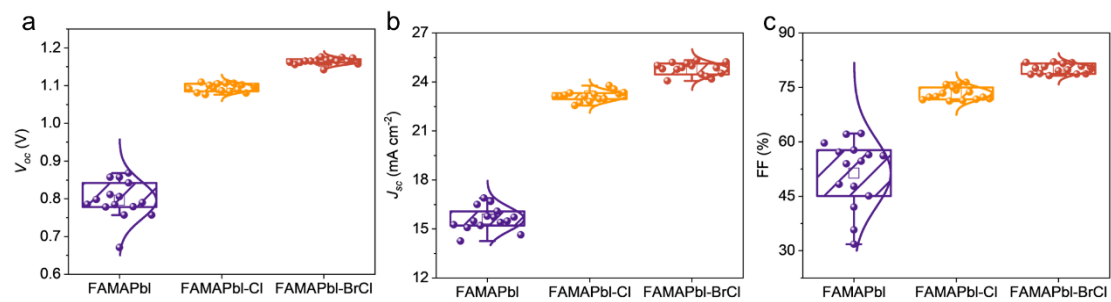


Figure S32. a. V_{oc} b. J_{sc} c. FF statistical distribution of PSCs fabricated by thermal evaporation-spin method.

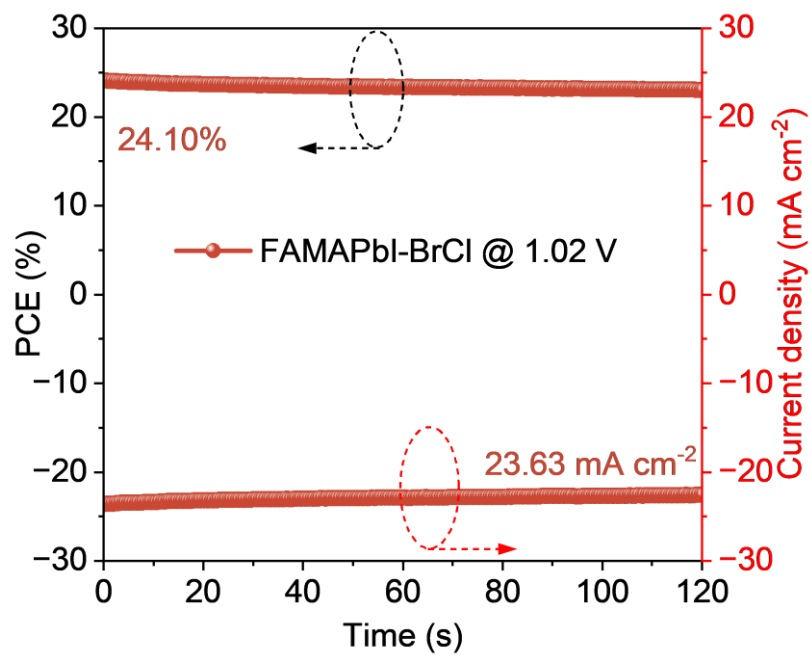


Figure S33. Typical steady-state power output at the initial maximum power point based on the FAMAPbI-BrCl perovskite devices fabricated by thermal evaporation-spin method.

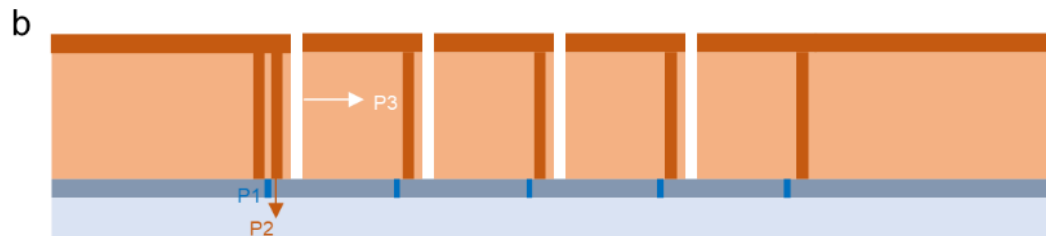
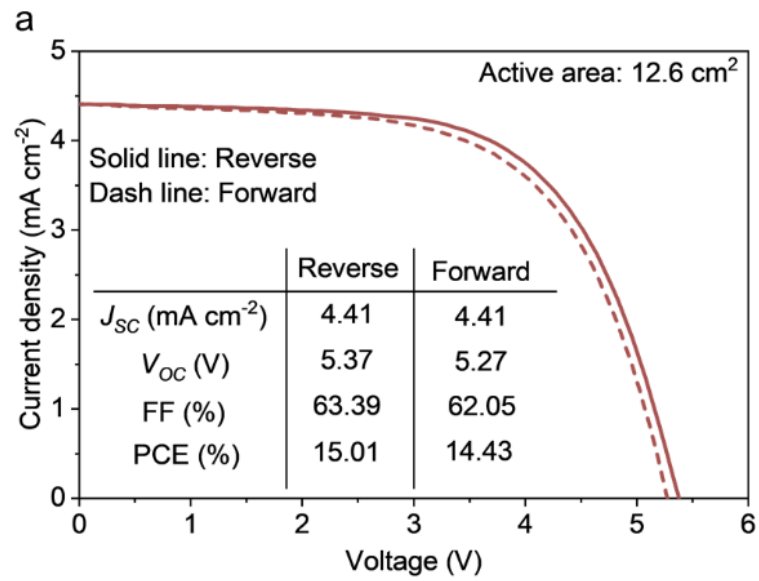


Figure S34. a. J - V curve of large-area module based on the FAMAPbI-BrCl. **b.** the structure of the perovskite solar cell module.

Table S3. Fitting parameters of the bi-exponential decay function of TRPL measurement based on the FAMAPbI, FAMAPbI-Cl, and FAMAPbI-BrCl perovskite films, respectively.

Sample	y₀	A₁	τ_1 (ns)	A₂	τ_2 (ns)	τ_{avg} (ns)	χ^2 (10⁻⁵)
FAMAPbI	0.017	0.801	2.341	0.124	77.422	12.406	6.705
FAMAPbI-Cl	0.023	0.106	68.062	0.831	317.309	289.112	30.177
FAMAPbI- BrCl	0.008	0.055	48.256	0.850	482.176	455.805	35.206

Table S4. A list of recently reported perovskite solar cells with high efficiency that fabricated with two-step thermal evaporation PbI₂-scalable solution deposition methods (including spray, inject printing, and blade deposition methods).

Year	methods	J_{SC} (mA/cm²)	V_{oc} (V)	FF (%)	PCE (%)	Ref
2017	thermal evaporation -spray	12.82	0.969	50.39	6.26	1
2017	thermal evaporation -inject printing	-	-	-	6.10	2
2019	thermal evaporation -spray	12	1	80	10.0	3
2021	thermal evaporation -blade	23.31	1.11	72.00	18.7	4
2021	thermal evaporation -spray	22.73	1.065	79.1	19.17	5
2022	thermal evaporation -inject printing	22.86	1.016	78.7	18.26	6
2023	thermal evaporation -spray	20.33	1.17	81.6	19.42	7
2023	thermal evaporation -blade	24.06	1.10	74.59	19.8	8
2024	thermal evaporation-blade	25.03	1.12	79.12	22.22	This work

Table S5. Photovoltaic parameters of devices fabricated by thermal evaporation-blade method based on the FAPbI-BrCl.

Device	Direction	V_{oc} (V)	J_{sc} (mA/cm²)	FF (%)	PCE (%)
	Reverse	1.10	24.26	76.60	20.37
FAPbI-BrCl	Forward	1.10	24.19	75.81	20.10
	Average	1.08±0.02	23.10±0.82	70.81±4.26	17.63±1.69

Table S6. Photovoltaic parameters of devices fabricated by thermal evaporation-spin method based on the FAMAPbI, FAMAPbI-Cl, and FAMAPbI-BrCl, respectively.

Device	Direction	V_{oc} (V)	J_{sc} (mA/cm ²)	FF (%)	PCE (%)
FAMAPbI	Reverse	0.778	16.90	54.64	8.82
	Forward	0.950	17.01	54.59	7.19
	Average	0.796±0.050	15.61±0.72	51.36±9.35	6.36±1.15
FAMAPbI-Cl	Reverse	1.101	23.77	75.00	19.67
	Forward	1.099	23.79	71.75	18.76
	Average	1.094±0.011	23.14±0.31	73.28±1.80	18.55±0.58
FAMAPbI-BrCl	Reverse	1.176	25.33	82.03	24.43
	Forward	1.175	25.16	80.54	23.82
	Average	1.164±0.008	24.78±0.39	80.12±1.33	23.11±0.66

Table S7. A list of recently reported inverted perovskite solar cells with high efficiency that fabricated with thermal evaporation-spin deposition method.

Year	Perovskite	J_{sc} (mA/cm ²)	V_{oc} (V)	FF (%)	PCE (%)	Ref
2016	FA _{1-x} MA _x PbI _{3-y} Br _y	18.26	0.99	68.6	12.41	9
2017	MAPbI ₃	19.1	1.116	75.4	16.10	10
2018	MAPbI ₃	19.9	1.116	75.7	16.80	11
2018	MAPbI ₃	22.18	0.915	73.8	16.85	12
2020	MAPbI _{3-x-y} Br _x Cl _y	21.2	1.15	81.7	19.80	13
2021	Cs _x FA _y MA _{1-x-y} PbI _{3-z} Br _z	19.59	1.082	80.34	17.03	14
2022	Cs _x FA _y MA _{1-x-y} PbI _{3-z} Br _z	23.19	1.14	80.6	21.31	15
2023	Cs _x FA _y MA _{1-x-y} PbI _{3-z} Br _z	20.9	1.19	81.6	20.3	16
2023	Cs _x FA _y MA _{1-x-y} PbI _{3-z} Br _z	23.90	1.11	79.50	21.06	17
2023	Cs _x FA _{1-x} PbI _{3-y} Br _y	-	-	-	19.5	18
2023	Cs _x FA _y MA _{1-x-y} PbI ₃	21.84	1.16	79.96	20.3	19
2024	FA_{1-x}MA_xPbI_{3-y}Br_y	25.33	1.176	82.03	24.43	This work

Table S8. A list of recently reported $5 \times 5 \text{ cm}^2$ perovskite solar modules with high efficiency that fabricated with two-step sequential deposition method.

Year	J_{sc} (mA/cm²)	V_{oc} (V)	FF (%)	PCE (%)	Ref
2019	3.70	5.26	66.11	12.86	20
2020	2.62	6.19	68.00	11.07	21
2020	3.47	6.71	71.00	16.54	22
2021	7.31	2.96	67.23	14.55	23
2023	4.51	5.33	68.37	16.42	24
2024	4.41	5.37	63.39	15.01	This work

References

1. G. Chai, S. Wang, Z. Xia, S. Luo, C. Teng, T. Yang, Z. Nie, T. Meng and H. Zhou, *Semicond Sci Technol*, 2017, **32**, 074003.
2. T. Abzieher, F. Mathies, M. Hetterich, A. Welle, D. Gerthsen, U. Lemmer, U. W. Paetzold and M. Powalla, *Phys. Status Solidi*, 2017, **214**, 1700509.
3. L. Cojocar, K. Wienands, U. Erdil, P. S. C. Schulze, L. E. Mundt, A. J. Bett, M. Breitwieser, F. Lombeck, M. Prescher, L. Kirste, S. Vierrath, J. C. Goldschmidt and S. W. Glunz, *IEEE J. Photovolt.*, 2020, **10**, 276-286.
4. S. Siegrist, S. C. Yang, E. Gilshtein, X. Sun, A. N. Tiwari and F. Fu, *J. Mater. Chem. A*, 2021, **9**, 26680-26687.
5. X. Yu, J. Li, Y. Mo, T. Xiang, Z. Ku, F. Huang, F. Long, Y. Peng and Y.-B. Cheng, *J. Energy Chem.*, 2022, **67**, 201-208.
6. H. Yang, J. Wang, X. Yu, Y. Feng, X. Chen, F. Long, Z. Ku, F. Huang, Y. Cheng and Y. Peng, *Chem. Phys. Lett*, 2022, **807**, 140084.
7. X. Chen, C. Geng, X. Yu, Y. Feng, C. Liang, Y. Peng and Y.-b. Cheng, *Mater. Today Energy*, 2023, **34**, 101316.
8. J. Fang, D. Lin, W. Huang, X. Wang, H. Li, S. Li, G. Xie, D. Wang and L. Qiu, *J. Alloys Compd.*, 2023, **955**, 170255.
9. J. Xi, Z. Wu, K. Xi, H. Dong, B. Xia, T. Lei, F. Yuan, W. Wu, B. Jiao and X. Hou, *Nano Energy*, 2016, **26**, 438-445.
10. F. Fu, T. Feurer, Thomas P. Weiss, S. Pisoni, E. Avancini, C. Andres, S. Buecheler and Ayodhya N. Tiwari, *Nat. Energy*, 2016, **2**, 16190.
11. F. Fu, S. Pisoni, T. P. Weiss, T. Feurer, A. Wackerlin, P. Fuchs, S. Nishiwaki, L. Zortea, A. N. Tiwari and S. Buecheler, *Adv. Sci.*, 2018, **5**, 1700675.
12. T. Lei, H. Dong, J. Xi, Y. Niu, J. Xu, F. Yuan, B. Jiao, W. Zhang, X. Hou and Z. Wu, *Chem. Commun.*, 2018, **54**, 6177-6180.

13. W. Soltanpoor, C. Dreessen, M. C. Sahiner, I. Susic, A. Z. Afshord, V. S. Chirvony, P. P. Boix, G. Gunbas, S. Yerci and H. J. Bolink, *ACS Appl. Energy Mater.*, 2020, **3**, 8257-8265.
14. Y. Li, B. Shi, Q. Xu, L. Yan, N. Ren, Y. Chen, W. Han, Q. Huang, Y. Zhao and X. Zhang, *Adv. Energy Mater.*, 2021, **11**, 2102046.
15. L. Mao, T. Yang, H. Zhang, J. Shi, Y. Hu, P. Zeng, F. Li, J. Gong, X. Fang, Y. Sun, X. Liu, J. Du, A. Han, L. Zhang, W. Liu, F. Meng, X. Cui, Z. Liu and M. Liu, *Adv. Mater.*, 2022, **34**, 2206193.
16. X. Luo, H. Luo, H. Li, R. Xia, X. Zheng, Z. Huang, Z. Liu, H. Gao, X. Zhang, S. Li, Z. Feng, Y. Chen and H. Tan, *Adv. Mater.*, 2023, **35**, 2207883.
17. A. Z. Afshord, B. E. Uzuner, W. Soltanpoor, S. H. Sedani, T. Aernouts, G. Gunbas, Y. Kuang and S. Yerci, *Adv. Funct. Mater.*, 2023, **33**, 2301695.
18. X. Y. Chin, D. Turkay, J. A. Steele, S. Tabean, S. Eswara, M. Mensi, P. Fiala, C. M. Wolff, A. Paracchino, K. Artuk, D. Jacobs, Q. Guesnay, F. Sahli, G. Andreatta, M. Boccard, Q. Jeangros and C. Ballif, *Science*, 2023, **381**, 59-63.
19. F. Zhang, B. B. Tu, S. F. Yang, K. Fan, Z. L. Liu, Z. J. Xiong, J. Zhang, W. Li, H. T. Huang, C. Yu, A. K. Y. Jen and K. Yao, *Adv. Mater.*, 2023, **35**, 2303139.
20. F. Matteocci, L. Vesce, F. U. Kosasih, L. A. Castriotta, S. Cacovich, A. L. Palma, G. Divitini, C. Ducati and A. Di Carlo, *ACS Appl. Mater. Interfaces*, 2019, **11**, 25195-25204.
21. Z. Huang, X. Hu, Z. Xing, X. Meng, X. Duan, J. Long, T. Hu, L. Tan and Y. Chen, *J. Phys. Chem. C*, 2020, **124**, 8129-8139.
22. J. Zhang, T. Bu, J. Li, H. Li, Y. Mo, Z. Wu, Y. Liu, X.-L. Zhang, Y.-B. Cheng and F. Huang, *J. Mater. Chem. A*, 2020, **8**, 8447-8454.
23. G. Tong, D. Y. Son, L. K. Ono, Y. Liu, Y. Hu, H. Zhang, A. Jamshaid,

- L. Qiu, Z. Liu and Y. Qi, *Adv. Energy Mater.*, 2021, **11**, 2003712.
24. J. He, W. Sheng, J. Yang, Y. Zhong, Y. Su, L. Tan and Y. Chen, *Energy Environ. Sci.*, 2023, **16**, 629-640.